International Journal of Solids and Structures 191–192 (2020) 87–98

Contents lists available at ScienceDirect

International Journal of Solids and Structures

journal homepage: www.elsevier.com/locate/ijsolstr

# How variability in interfacial properties results in tougher bonded composite joints by triggering bridging

Xiaole Li[a], Ran Tao[a], Marco Alfano[b], Gilles Lubineau[a,*]

[a] *King Abdullah University of Science and Technology (KAUST), Physical Sciences and Engineering Division (PSE), COHMAS Laboratory, Thuwal 23955-6900, Saudi Arabia*

[b] *Department of Mechanical, Energy and Management Engineering, University of Calabria, Rende 87036, CS, Italy*

ARTICLE INFO

*Article history:*
Received 10 September 2019
Revised 11 November 2019
Accepted 22 November 2019
Available online 27 November 2019

*Keywords:*
Composite joints
Stochastic cohesive zone model
Crack-tip transfer
Bridging ligament
Bondline thickness

ABSTRACT

Toughening strategies are needed to design high performance secondary bonded joints. Although adhesively bonded joints present a promising solution for cost-saving assembly, they are however among the most vulnerable parts in composite structures. Due to the inherent heterogeneity of composite substrates and the infeasibility of ideal surface pretreatments, the bonding properties of composite joints feature a spatial variability that can result in a wide variety of debonding phenomenology, such as crack tip transfer, crack bifurcation or ligament bridging. In the present work, we apply a cohesive zone model with spatially stochastic interfacial properties to model the physical behaviors that take place during debonding of an adhesively bonded composite joint. The joint distribution of the two essential bonding properties, namely, the critical separating stress $\sigma_m$ and the strain energy release rate $G_c$, follows a bivariate lognormal probability distribution. The proposed model captures the mechanisms of crack-tip transfer and the failure of bridging adhesive ligaments between the composite adherends, as well as the associated toughening of joints. We find that the extrinsic dissipation attributed to extra debonding areas and plastic-damage mechanisms of ligaments may be one of the primary causes for the thickness effect of bondline on the fracture toughness, commonly observed for adhesively bonded joints. Through a parametric study, we discuss the effect of variability in interfacial properties on the enhancement of toughness of bonded composite joints. The outcomes of this work may provide insights into the fundamental failure mechanisms of secondary bonded composite joints.



## 1. Introduction

The performance of composite joints is a major limiting factor in the structural integrity and potential wider applications of composite structures. In general, there are two main approaches to assemble Fiber Reinforced Polymer (FRP) composites: adhesive bonding and mechanical fastening. In contrast to bolted joints, adhesively bonded joints (ABJs) feature more homogeneous stress distribution, enable the design of complex yet light structures, and are beneficial for fatigue resistance and service lifetime. These positive characteristics make ABJs a promising approach for future composite assembly (Budhe et al., 2017; Katnam et al., 2013). However, the relatively weak bonding properties of ABJs have impeded the development of secondary bonding. Also, the failure of ABJs is sometimes brittle, which limits the confidence of designers in using such technological solution. Crack arrest features are still needed to ensure the integrity of structure and a more progressive failure. As a consequence, secondary bonding is rarely used alone today, but rather used jointly with bolted or riveted junctions. The challenge now is to move to integral or almost integral (few rivets) secondary bonding solutions. Such a move requires more advanced strategies for improving the toughness of ABJs and conferring them a more progressive damage behavior.

Significant efforts have been made to improve the performance of ABJs, either through advanced chemistry of the adhesive materials (Moszner and Salz, 2007) or by tailoring the topology of the adhesive layer (Heide-Jrgensen et al., 2018; Garca-Guzmn et al., 2018; Maloney and Fleck, 2019) and substrates (Maloney and Fleck, 2018; Nguyen et al., 2016). Surface preparation (Wingfield, 1993) is one of the most essential steps. Pretreatment of the adherend surface is the most fundamental requirement to remove contaminants composed of low energy and friable materials, *e.g.*, mould release agents, which often have adverse effects on adhesion (Tao et al., 2018). Pretreatment of the substrate surface to be bonded can chemically fully reactivate the surface and thus

* Corresponding author.
*E-mail address:* gilles.lubineau@kaust.edu.sa (G. Lubineau).

https://doi.org/10.1016/j.ijsolstr.2019.11.021
0020-7683/

establish good adhesion. Different techniques are developed to pretreat a substrate, such as peel-ply preparation, grit blasting, etching, laser treatment, plasma treatment *etc*. Different trends in the toughening effects for different surface treatments and different enhanced performances of bonded FRP joints were demonstrated (Moyer and Wightman, 1991). Recently, the most commonly used pretreatment techniques, *i.e*., the peel-ply pretreatment, sandblasting and pulsed laser irradiation, were evaluated experimentally by Tao et al. (2018), which showed that the mechanisms that contribute to the toughening effects incurred by different techniques of surface pretreatment are different.

The inherent heterogeneity of FRP composites leads to a non-uniform topology of substrate surfaces. Different pretreatment techniques may enhance or mitigate this non-uniformity to some extent (Prolongo et al., 2010; Tzetzis, 2008), thus giving FRP joints with different bonding performances. Moreover, in industrial settings, it is impossible to perfectly control the quality of surface pretreatment, *e.g*., the irradiation energy of laser ablation, and thus the morphology of the bonding surface cannot be guaranteed to be ideally homogeneous and mechanically sound. Overall, imperfections ultimately lead to variability in interfacial properties around the nominal values, namely, the stochastic characteristics in adhesion of FRP joints. This may be the essential cause of the phenomenon whereby, in some scenarios, debonding transfers randomly from one interface to the other, thus building up adhesive ligaments that span the crack and bridge the adherends (Tenchev and Falzon, 2007; Sills and Thouless, 2015). Of course, variability in bonding properties might also be attributed to inherent surface defects in pregreg due to the fabrication process. Several studies have focused on the overall mechanical response of materials (Dimas et al., 2016, 2015, 2014) or interface (Taleb Ali et al., 2018; Xu et al., 2014; Motamedi et al., 2013; Khokhar et al., 2009, 2013; Jumel, 2017) subjected to propertys heterogeneity induced by cracks, defects, or other types of flaws, and it was found that the material or bonding strengths are sensitive to randomly distributed properties. Particularly, a toughening of material attributed to the spatial heterogeneity in material properties has been observed (Dimas et al., 2016). Tao et al. (2019) carried out an *in-situ* analysis on debonding of FRP ABJs. Diverse failure mechanisms were observed from the specimens after different pretreatment techniques, *e.g*., ligament stretching for laser ablation and adhesive nesting for sandblasting. The *in-situ* observations revealed that the heterogeneous bonding surface induced by the randomly distributed exposed fibers is possibly the main trigger of adhesive fabrications and adhesive ligaments. This study confirms that the variability in substrates morphology may have an effect on the debonding behaviors and, in some cases, may significantly enhance the bonding performance of composite joints.

The adhesive ligament is a phenomenon that is analogous to the fiber bridging regularly observed in laminate delamination. Fiber bridging is a typical mechanism due to variability in the material properties induced by micro effects, *e.g*., weak bonding and fiber misalignments (Kaute et al., 1993). Canal et al. (2017, 2016) applied connector elements with randomly distributed strong and weak strengths along the crack path to reproduce microscale imperfections and explore the mechanisms of fiber bridging. They found that the property randomness eases the formation of large bridging zones, which decreases the stress level at the crack tip and considerably improves the crack growth resistance, thus giving rise to the enhancement of fracture toughness observed in many experimental works (Mirzaei et al., 2016; Manshadi et al., 2014). Similarly, the stretched ligaments alter the structural response by exerting a closure force and thus easing the stress field around the crack-tip area. Moreover, the extrinsic dissipation, such as the dissipation from plastic deformation and failure of ligaments, may enhance the joints resistance to cracks. All such comprehensive failure mechanisms due to property randomness and the associated toughening effect for composite joints are of particular interest. Currently, an in-depth understanding of these mechanisms is still challenging due to the lack of an effective computational tool and successful experimental means.

The objective of this work is to thoroughly clarify the influence of variability in interfacial properties on the performance of FRP ABJs. We investigate the fundamental mechanisms of crack-tip transfer and bridging adhesive ligaments, which can shed light on the essence of the toughening effect arising from the variabilities in interfacial properties. We demonstrate the potential of interface patterning to trigger extrinsic dissipation. This paper is organized as follows: firstly, we propose a modeling strategy based on Cohesive Zone Model (CZM) with spatially stochastic interfacial properties, for the purpose of capturing the various physical mechanisms that occur during damage of the secondary bonded composite joints. After validating the model, we apply the model as an exploration tool to elucidate the role of the bondline thickness on the global toughening effects in FRP joints. Finally, we perform a sensitivity study of the bonding performance of the FRP joint to the statistical characteristics of properties.

## 2. A modeling strategy for adhesively bonded FRP joints

Based on CZM, several stochastic models have been developed to analyze the mechanical response of ABJs subjected to spacial variations (Xu et al., 2014; Jumel, 2017; Ashcroft et al., 2012) and temporal variations (Meng and Thouless, 2019) in bonding properties. However, most of those works only consider the randomness of the Strain Energy Release Rate (SERR) $G_c$. To characterize the debonding behavior of ABJs, an accurate determination of the two properties, separating stress $\sigma_m$ and SERR $G_c$, is crucial. Moreover, all the existing models deploy a single layer of cohesive elements, which do not discriminate between cohesive failure and interfacial failure. This simplified description of the adhesive layer also impedes the proper description of some key mechanisms, including ligament creation and subsequent bridging. Thus a detailed comprehension of local failure mechanisms is then compromised. It is generally believed that $\sigma_m$ and $G_c$ are statistically dependent variables. (Xu et al., 2014) considered $\sigma_m$ to be proportional to the square root of the random $G_c$, implying a perfect positive correlation between $\sigma_m$ and $G_c$. With a measurement of crack-tip opening and an analytical solution in the framework of J-integral, one can experimentally extract the traction-separation law and thus obtain $\sigma_m$ and $G_c$ (Gowrishankar et al., 2012; Wu et al., 2016; Sarrado et al., 2016; Blaysat et al., 2015). But such approaches are heavily influenced by the difficulty of measuring local crack-tip opening (Monsef et al., 2019). Recently, Wu et al. (2019) proposed an approach to simultaneously extract mixed mode traction-separation laws with the remotely applied load and displacement and rotation of load points, which facilitates the measurement of traction-separation laws. Here, we propose a practical modeling strategy, which deploys two layers of cohesive elements with the stochastic ($\sigma_m$, $G_c$) following a joint probability distribution, to model FRP joints in detail, thus elucidating the role of variability of interfacial properties on the ABJs performance.

### 2.1. Joint probability distribution function (PDF) of ($\sigma_{m,}$ $_{G_c)}$

The first step is to choose an appropriate representation of the PDF. Gaussian distribution, with a simple mathematical form, is commonly employed to describe the randomness of material properties. However, the Gaussian distribution has a left tail that extends to negative infinity, and thus is not suitable in this case as no bonding properties can be negative. Therefore, the bonding properties should statistically follow a non-negative skewed distribu-

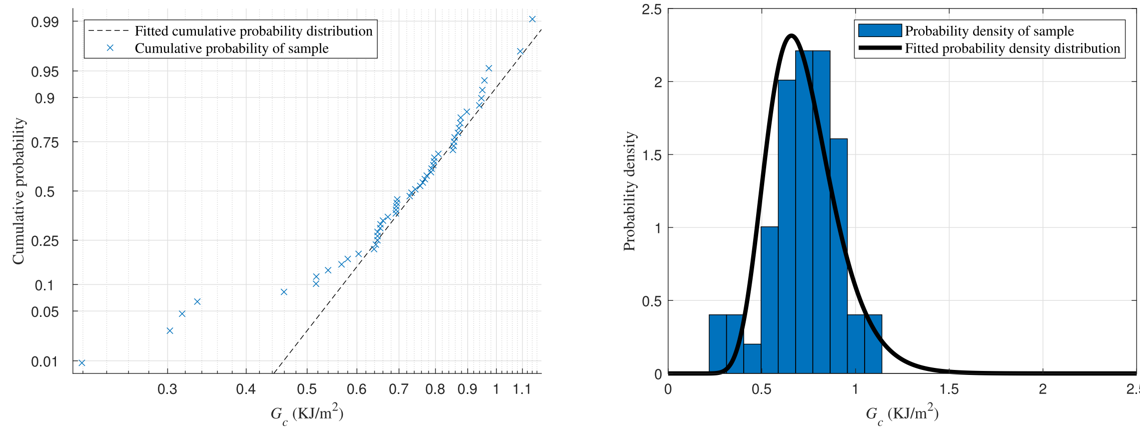


(a) (b)

**Fig. 1.** Statistical results of a site-specific sample of $G_c$ comparing to the corresponding distribution fits estimated by MLE. (a) Cumulative probability distribution and (b) Probability density distribution. The data are extracted from a previous work in which double cantilever tests have been performed using laser-treated M21/T700 FRP laminates as substrates and Araldite® 420 epoxy as adhesives and refer to the publication (Tao et al., 2018) for more details.

tion. By using a joint lognormal distribution of the stiffness and strength, Dimas et al. (2016) analytically demonstrated the toughening mechanism for materials with spatially random material heterogeneities. For lognormal distribution, the Napierian logarithm is regarded as the random variable and is considered to be be normally distributed. This ensures that the real variables (here the interface properties) take only positive real values. Fig. 1a shows the cumulative probability of an available sample of $G_c$ compared to a fitted lognormal distribution based on the same sample via Maximum Likelihood Estimation (MLE). The sample includes 54 raw laboratory measurements of $G_c$ from the composite joint specimen whose substrate surfaces are pretreated with laser ablation. Fig. 1b compares the probability density distribution of the sample and the classical lognormal distribution whose parameters are estimated by MLE. It is evident that the lognormal distribution adequately describes the statistical characteristics of the bonding properties of FRP joints.

For simplicity, we consider that both the variables $\sigma_m$ and $G_c$ follow lognormal PDFs:

$$\begin{aligned}(\sigma_m) &\sim \mathrm{Lognormal}(\mu_\sigma, d_\sigma)\\ (G_c) &\sim \mathrm{Lognormal}(\mu_G, d_G)\end{aligned} \tag{1}$$

in which $\mu_\sigma$ and $\mu_G$ are the expectations of the logarithms of random variables, $d_\sigma$ and $d_G$ are the standard deviations of (ln($\sigma_m$), ln($G_c$)). These parameters can be obtained if the arithmetic mean E[$x$] and the arithmetic variance Var[$x$] of random variables are known (Balakrishnan and Lai, 2009):

$$\begin{aligned}\mu_\sigma &= \ln\left(\frac{\mathrm{E}[\sigma_\mathrm{m}]^2}{\sqrt{\mathrm{Var}[\sigma_\mathrm{m}]+\mathrm{E}[\sigma_\mathrm{m}]^2}}\right),\ (d_\sigma)^2 = \ln\left(1+\frac{\mathrm{Var}[\sigma_\mathrm{m}]}{\mathrm{E}[\sigma_\mathrm{m}]^2}\right)\\ \mu_G &= \ln\left(\frac{\mathrm{E}[G_\mathrm{c}]^2}{\sqrt{\mathrm{Var}[G_\mathrm{c}]+\mathrm{E}[G_\mathrm{c}]^2}}\right),\ (d_G)^2 = \ln\left(1+\frac{\mathrm{Var}[G_\mathrm{c}]}{\mathrm{E}[G_\mathrm{c}]^2}\right)\end{aligned} \tag{2}$$

As mentioned previously, $\sigma_m$ and $G_c$ are dependent variables. Considering the distribution for $\sigma_m$ and $G_c$ shown in Eq. (1), the dependent variables ($\sigma_m$, $G_c$) can be described by a bivariate lognormal PDF. The correlation coefficient $\rho$ quantifies the strength of the statistical relevance between $\sigma_m$ and $G_c$. The joint PDF of ($\sigma_m$, $G_c$) has the following form expressed with the parameters $\mu_\sigma$, $\mu_G$, $d_\sigma$, $d_G$, and $\rho$:

$$P_b(\sigma_m, G_c) = \frac{1}{2\pi d_\sigma d_G \sigma_\mathrm{m} G_\mathrm{c}\sqrt{1-\rho^2}} \exp\left(-\frac{A^2+B^2+2\rho AB}{2\left(1-\rho^2\right)}\right),\quad \sigma_\mathrm{m}, G_\mathrm{c} \in (0, +\infty) \tag{3}$$

in which

$$A = \frac{\ln(\sigma_\mathrm{m}) - \mu_\sigma}{d_\sigma} \text{ and } B = \frac{\ln(G_\mathrm{c}) - \mu_G}{d_G} \tag{4}$$

To estimate the parameters in the joint PDF, MLE can be performed once a joint sampling of the bivariate variable ($\sigma_m$, $G_c$) including $n$ observations is drawn. The likelihood function of the bivariate lognormal distribution is as follow:

$$L(\mu_\sigma, \mu_G, d_\sigma, d_G, \rho; data) = \prod_{i=1}^{n} P_b\left(\mu_\sigma, \mu_G, d_\sigma, d_G, \rho; data(\sigma_{m}, G_c)^i\right) \tag{5}$$

The parameters to be estimated can be straightforwardly obtained by maximizing the above likelihood function based on the sample (Cheng, 1986):

$$\hat{\mu}_\sigma = \frac{\sum_{i=1}^{n}\ln\left(\sigma_m^i\right)}{n},\quad \left(\hat{d}_\sigma\right)^2 = \frac{\sum_{i=1}^{n}\left(\ln\left(\sigma_m^i\right) - \hat{\mu}_\sigma\right)^2}{n-1} \tag{6}$$

$$\hat{\mu}_G = \frac{\sum_{i=1}^{n}\ln\left(G_c^i\right)}{n},\quad \left(\hat{d}_G\right)^2 = \frac{\sum_{i=1}^{n}\left(\ln\left(G_c^i\right) - \hat{\mu}_G\right)^2}{n-1} \tag{7}$$

$$\rho = \frac{\sum_{i=1}^{n}\left(\ln\left(\sigma_m^i\right) - \hat{\mu}_\sigma\right)\left(\ln\left(G_c^i\right) - \hat{\mu}_G\right)}{(n-1)\hat{d}_G\hat{d}_\sigma} \tag{8}$$

### 2.2. Modeling strategy using stochastic CZM

The two-dimensional CZM is used for modeling the interfacial failure during debonding of ABJs, the constitutive relationship of which is expressed as:

$$t_i(\delta_i) = \begin{cases} K\delta, & \delta_i < \delta_i^0 \\ (1-d)K\delta, & \delta_i^0 < \delta < \delta_i^f \\ 0, & \delta_i^f < \delta \end{cases} \tag{9}$$

where $K$ is the stiffness of the interface, $d$ is the damage variable to drive the interface degradation, $\delta_i$ is the separation between two bonded surfaces, and subscript $i$ indicates the crack mode. The classic quadratic stress criterion and the mode-independent evolution criterion are used to determine the initiation of the interfacial failure and crack propagation. The two criteria read:

$$\left(\frac{\sigma^1}{\sigma_m^1}\right)^2 + \left(\frac{\sigma^2}{\sigma_m^2}\right)^2 = 1 \tag{10}$$

$$\frac{G_\mathrm{dissipated}}{G_c} = 1 \tag{11}$$

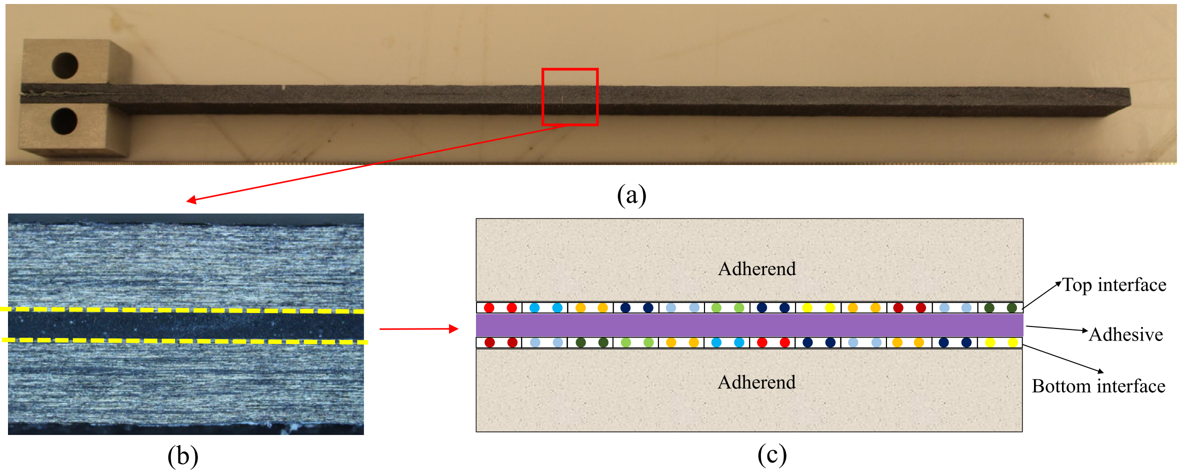


**Fig. 2.** A schematic illustration of the proposed strategy for modeling ABJs with variability in interfacial properties. (a) A FRP joint, (b) The mophology of cross-section of the joint and (c) The proposed modeling scheme.

The damage variable $d$ for a bilinear constitutive relationship read:

$$d = \frac{\delta_e^f\left(\delta_e - \delta_e^0\right)}{\delta_e\left(\delta_e^f - \delta_e^0\right)} \tag{12}$$

in which, $\delta_e^0$ and $\delta_e^f$ are the equivalent separations corresponding to the onset and completion of interfacial failure. The equivalent separation is calculated by $\delta_e = \sqrt{\delta_1^2 + \delta_2^2}$. The final separation $\delta_e^f$ is determined through:

$$\int_0^{\delta_e^f} t_e \mathrm{d}\delta_e = G_c \tag{13}$$

in which the equivalent traction is calculated as $t_e = \sqrt{t_1^2 + t_2^2}$. In the present model, $\left(\sigma_m^1 = \sigma_m^2, G_c\right)$ are the spatially stochastic variables that are designed to follow the bivariate lognormal distribution expressed in Eq. (3).

There are two physical interfaces for the bondline of ABJs, as highlighted by the dashed lines in Fig. 2. A variety of failure modes, *e.g.*, adhesive failure, cohesive failure and hybrid failure, can occur in ABJs (Zotti et al., 2016). As mentioned previously, the bondline is conventionally modeled by a single layer of cohesive elements, with which the apparent debonding performance and the overall response of joints can be studied. Nonetheless, this modeling scheme of the bondline may fail to capture the different failure modes and to elaborate on the local debonding mechanisms. The focus of this paper is on the essence of crack-tip transfer and ligament bridging during debonding, which is a mechanism attributed to the interaction of the two physical interfaces. Therefore, in the proposed modeling strategy, double layers of cohesive elements are modeled to characterize the bondline of a joint. Adhesive materials, such as epoxies, typically show an elastic-plastic-damage behavior (Haider et al., 2011); thus, the physically existing adhesive layer is modeled as an isotropic elastic-plastic-damage material. The modeling scheme is illustrated in Fig. 2c, in which different colors refer to the random interfacial properties. A script program was developed in the commercial software Matlab to complete the generation and assignation of stochastic interfacial properties.

## 3. Model validation

We simulated the Double Cantilever Beam (DCB) test, which is a standard test to measure mode-I SERR, to investigate the effect of variability in interfacial properties on bridging. The unidirectional laminated FRP substrate is stacked with Carbon/Epoxy M21/T700, whose properties are provided by the manufacturer and summarized in Table 1. The epoxy adhesive layer, whose thickness is $t_a = 0.10$ mm, is modeled as a classic elastic-plastic-damage medium, whose properties are also listed in Table 1. The configuration and geometrical parameters of the model are as shown in Fig. 3. The bonded region is discretized densely while a coarse mesh is adopted in other regions.

The parameters, $\mu_G$, and $d_G$ were estimated through MLE, as expressed in Eq. (7), based on the available sample of $G_c$. Then using Eq. (2) the estimations of the mean $\mathrm{E}(G_c)$ and the standard deviation $\sqrt{\mathrm{Var}(G_c)}$ of $G_c$ were obtained. The mean $\mathrm{E}(\sigma_m)$ of $\sigma_m$ was estimated by trial and error based on the authors' previous experimental investigations (Tao et al., 2018, 2019). Because the sampling of $\sigma_m$ was not available, for simplicity, the standard deviation $\sqrt{\mathrm{Var}(\sigma_m)}$ of $\sigma_m$ was initially estimated based on the following assumption:

$$\frac{\sigma_m}{\mathrm{E}(\sigma_m)} = \sqrt{\frac{G_c}{\mathrm{E}(G_c)}} \tag{14}$$

Applying the above relationship, we generated a sample of $G_c$, including 100,000 data. We performed the MLE to estimate $d_G$ based on the generated sample, and then using Eq. (2) we found the $\sqrt{\mathrm{Var}\,(\sigma_m)}$. The statistical properties of the interface used in the initial model can be found in Table 1. A perfect positive correlation between $\sigma_m$ and $G_c$ was assumed, *i.e.*, $\rho$=1.

For each layer of the interfaces, the length of the cohesive element was controlled at 0.20 mm. In total, 706 cohesive elements were included in the model, with each layer including 353 cohesive elements. Correspondingly, 706 pairs of random ($\sigma_m$, $G_c$) were generated following the joint lognormal PDF in Eq. (3) and assigned to the cohesive elements. To demonstrate the models robustness, we performed thirty simulations subjected to the same stochastic characteristics of interfacial properties. Fig. 4 shows examples of the generated data of the stochastic bonding properties, with perfect positive correlations. Fig. 5 shows the differences between the cohesive elements of the top interface and the bottom interface, which are stochastic but oscillate around 0 ($x = 0$ corresponds to the original crack-tip). Under the current stochastic characteristics, we expect that the difference in bonding properties will contribute to triggering the crack tip transfer and the resultant ligament bridging.

**Table 1**
The material properties adopted in modeling the debonding of the adhesively bonded FRP DCB specimen.

| | | | | |
|---|---|---|---|---|
| Carbon/Epoxy lamina (M21/T700) | | | | |
| $E_{11}$ (MPa) | $E_{22}$ (MPa) | $E_{33}$ (MPa) | $\nu_{12} = \nu_{13} = \nu_{23}$ | $G_{12}$ (MPa) |
| 125000 | 7800 | 7800 | 0.33 | 5100 |
| Epoxy adhesive (Araldite® 420) (Haider et al., 2011) | | | | |
| $E$ (MPa) | $\nu$ | Yield stress (MPa) | Ultimate stress (Mpa) | Fracture energy (KJ/m$^2$) |
| 1500 | 0.33 | 27 | 37 | 0.22 |
| Stochastic interface | | | | |
| E($\sigma_m$) (MPa) | E($G_c$) (KJ/m$^2$) | $\sqrt{\text{Var}(\sigma_m)}$ | $\sqrt{\text{Var}(G_c)}$ | $\rho$ |
| 24 | 0.72 | 3.03 | 0.19 | 1.0 |

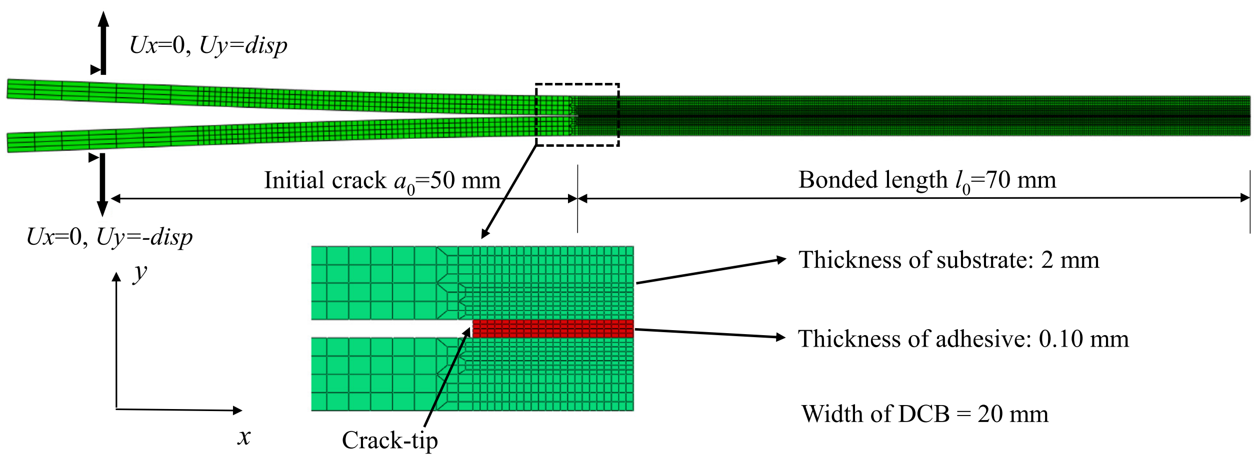


**Fig. 3.** Finite element model with geometrical parameters and boundary conditions. The loading points are fixed in $x$ direction and imposed displacement-controlled loading $P$ in $y$ direction.

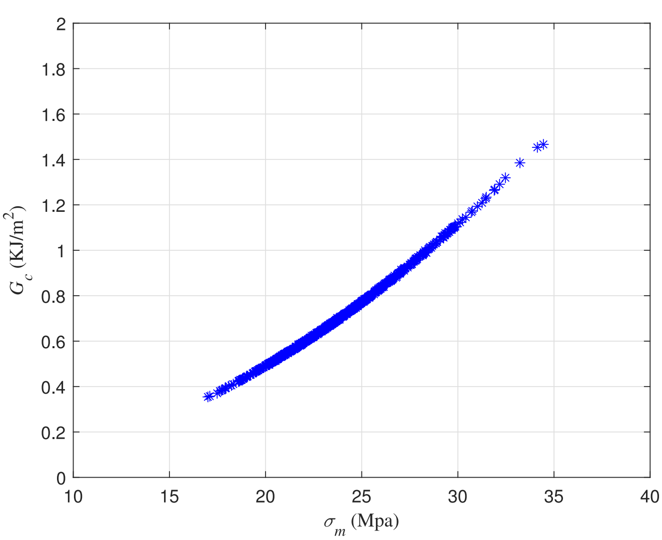


**Fig. 4.** Scatter plot of the generated sample pairs of $\sigma_m$ and $G_c$.

Fig. 6a presents a series of experimentally observed events during debonding of the FRP DCB specimen (Tao et al., 2018). The surfaces of bonded substrates were uniformly pre-treated along the direction of crack propagating via pulsed $CO_2$ laser irradiation. During debonding, the crack stopped advancing along its original interface and nucleated in the parallel interface below the initial one. This process is the so-called crack-tip transfer. Shortly after, an adhesive ligament, which spanned the crack, waked at a shallow angle. The adhesive ligament trapped between the two broken interfaces first deformed like a short beam, causing a strengthening of the beam arm stiffness, and eased the stress field around the crack tip. Afterward, the adhesive ligaments resulted from the crack-tip transfer experienced stretching and failure. For the $in-situ$ observations of failure ligament, readers can refer to (Tao et al., 2018). Note that in the second image of Fig. 6a, crack-tip transfer occurred again, and multiple ligaments were built up. The numerical model also captured similar behaviors, as shown in Fig. 6b. Failure profiles of the DCB substrate after detachment of the present segment showed multiple broken ligaments, and interphase or residues of the epoxy left on the FRP adherends, which undergoes plastic deformation, as shown in the last image of Fig. 6b, similar with experimental observations. All the above comparisons indicate that numerical simulation has demonstrated comparable debonding behaviors to these experiments, which prove the validity of the present model in capturing the physical mechanisms of crack-tip transfer and bridging adhesive ligaments.

In the following, simulations of the model with deterministic properties were also performed for comparison, referred to as the reference model. Fig. 7a shows the structural responses of five typical simulations with stochastic properties, as well as that of the reference models. The SERR and the associated R-curves, shown in Fig. 7b, were extracted using data reduction techniques (Berry, 1963). All five models behaves similarly. In contrast to the

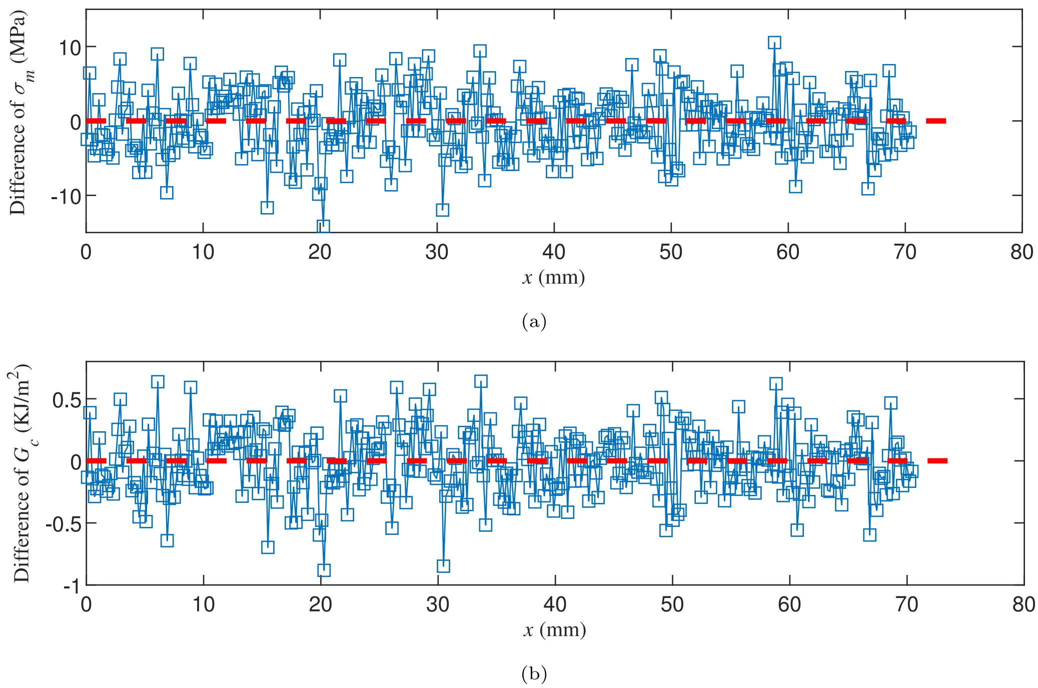


**Fig. 5.** Plot of the difference of (a) $\sigma_m$ and (b) $G_c$ for the corresponding cohesive elements of the top interface and bottom interface.

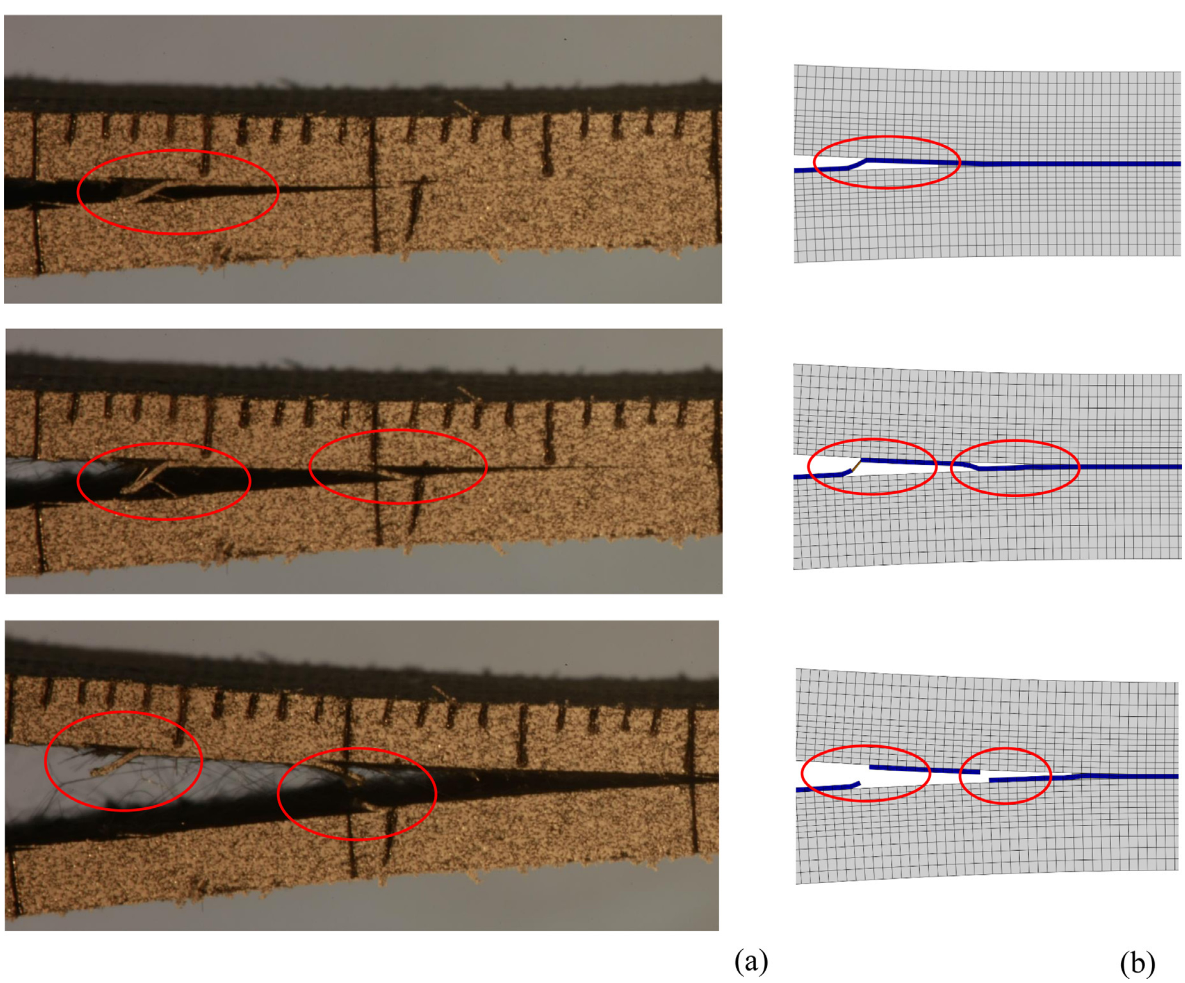


**Fig. 6.** The crack-tip transfer and ligament bridging observed in (a) Experiment and (b) Simulation with the stochastic CZM model. From top to bottom: Crack-tip transfer, ligament bridging, and multiple ligaments. The highlighted regions with red circles are the regions where crack-tip transfer and ligament bridging happens (bondline thickness $t_a = 0.10$ mm). (For interpretation of the references to color in this figure legend, the reader is referred to the web version of this article.)

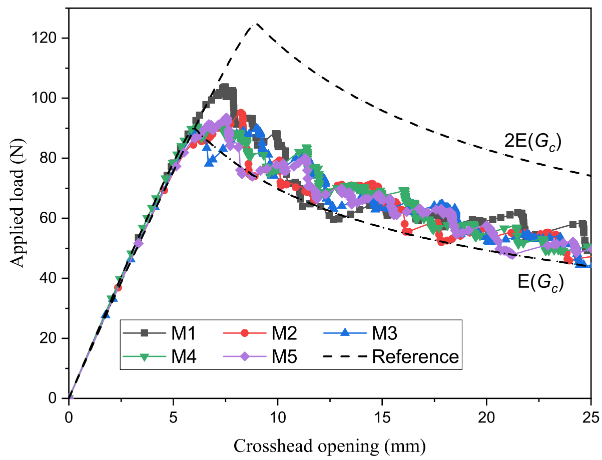


(a)

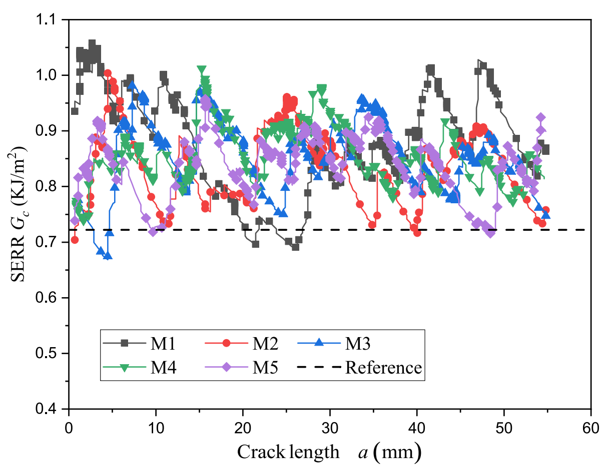


(b)

**Fig. 7.** The structure responses obtained by the present model with the comparison to the reference model. (a) Applied load *vs.* crosshead opening curve and (b) R-curve.

deterministic system, the spatial heterogeneity of the interfacial properties leads to oscillations in the structure responses, which demonstrates an instability due to the spatially distributed heterogeneity of interface properties. For the DCB in the presence of ligaments, the force applied on the beam arm is generally higher than that of the reference model with deterministic $G_c$ subjected to the same crack opening. As the crack opening increases, the ligaments start stretching, and they provide a shielding effect by exerting a substantial crack closure force, which features the response of joint with overshoot compared to the response curve from the reference model with E($G_c$), but lower than that of the reference model with 2E($G_c$). The adhesive ligaments significantly hinder crack propagation through elongation, giving rise to plastic deformation of the adhesives and approaching to the rupture strain. Meanwhile, extra debonding surfaces may also be introduced into the system during the stretching of ligaments. All these mechanisms contribute to increasing the amount of extrinsic dissipation in terms of additional debonding areas and plastic and fracture energy of adhesives, which has been demonstrated by the comparison of the obtained R-curves during the crack propagating from $\Delta a = 0$ mm to $\Delta a = 55$ mm, as shown in Fig. 7b. This shows an enhancement of approximately 16% in toughness compared to the reference model. The oscillation of the numerically measured SERR indicates the elongation and bulk fracture of the adhesive ligaments. The close resemblance of the numerical results from the five models with the same statistic parameters suggests that the model robustly captures the essential features of the phenomenon. A mismatch also occurs, which makes sense because, in this problem, the statistic properties are based on a large amount of data, and due to the limit of computational resources, only a limited number of simulations can be performed.

## 4. The effect of bondline thickness on the fracture toughness of FRP joints

Many tests have demonstrated significant bondline thickness effects on the performance of bonded joints, whereby the bonding toughness shows divergence as the bondline thickness is varied (Carlberger and Stigh, 2010; Azari et al., 2011; Ji et al., 2010; Marzi et al., 2011; Boutar et al., 2016; Ji et al., 2013). Considerable efforts have been made to interpret the reasons leading to this thickness effect (Ji et al., 2010; Liao et al., 2013; Arenas et al., 2010; Noda et al., 2007). A classic explanation is that the shape and size of plasticity zone within adhesive layer change with bondline thickness, and thus macroscopically joints demonstrate different toughness (Kinloch and Shaw, 1981). This can be the mechanism leading to the bondline thickness effect for cohesive fracture dominated joints. For the joints dominated by interfacial fracture, no or little plasticity is formed within adhesives. Crack-tip transfer and bridging ligaments may increase the joints toughness according to our analysis in the previous section, and it is worth exploring the origin of the variations in fracture toughness based on the thickness effect on the crack-tip transfer and bridging ligaments. This might be a key factor leading to the effect of bondline thickness on the joints toughness. We performed six groups of simulations, the bondline thicknesses of which were, respectively, $t_a = 0.10$, 0.12, 0.15, 0.20, 0.30, 0.50 mm. The adopted stochastic interface properties are in line with those listed in Table 1. Again, we generated at least thirty models for each group of simulations to achieve statistical convergence.

Fig. 8 shows the typical predictions obtained from the models with different bondline thicknesses. Explicit differences can be observed from the load-opening curves shown in Fig. 8a, as well as the R-curves shown in Fig. 8b. No ligaments were captured during the debonding of the model with baseline thickness of 0.50 mm. Thus, both the structural response and R-curves of this model gently oscillate around the result from the reference model, see Fig. 8a and b. The number of ligaments built up and the average $G_c$ during the crack propagating from $\Delta a = 0$ mm to $\Delta a = 55$ mm are plotted as a function of the bondline thickness in Fig. 8c, where we can see that the number of ligaments decreases monotonically with increasing bondline thickness, asymptotically approaching zero, while the $G_c$ increases monotonically as the thickness of the adhesive increases from 0.10 to about 0.20 mm. The model with $t_a = 0.20$ mm features the maximum $G_c$ compared to the other cases, which is around 20.6% higher than the reference value. At $t_a = 0.30$ mm, the average $G_c$ is considerably lower than that for the model with $t_a = 0.20$ mm, indicating that, under the current stochastic characteristics of interfacial properties, the fracture toughness of the joint reaches a maximum with a bondline thickness between 0.20 and 0.30 mm. It should be noted that, in the scenario of interfacial debonding, no or very little plasticity was developed within adhesive layer for our simulations. The above trends of toughness with bondline thickness agree with those of the existing experimental observations (Carlberger and Stigh, 2010; Boutar et al., 2016; Arenas et al., 2010).

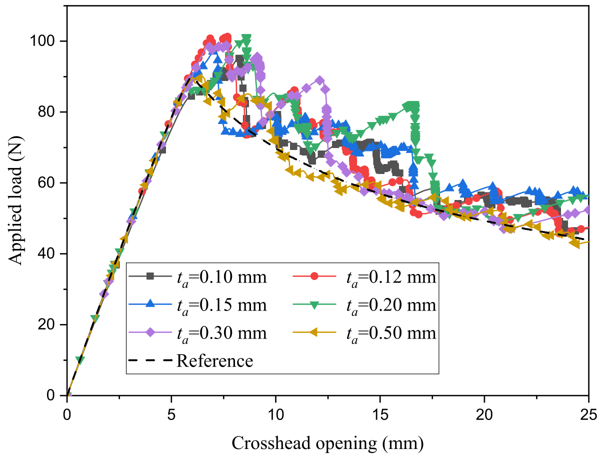


(a)

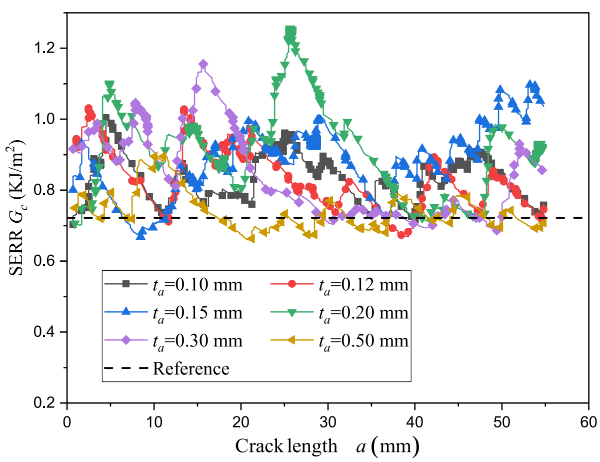


(b)

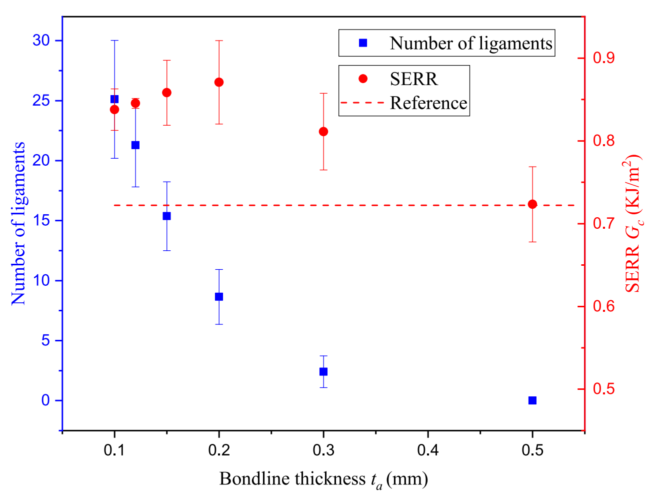


(c)

**Fig. 8.** The structure responses obtained by the present model with different bondline thickness $t_a$ with the comparison to the reference model. (a) Applied load *vs.* crosshead opening curve, (b) R-curve and (c) Scatter plot of ligament number and average SERR *vs.* bondine thickness.

The reason for this established trend is that an increase in dissipation due to the thickening of ductile ligaments and a reduction in the number of bridging ligaments compensate for each other. More specifically, when the bondline is relatively thin, the added dissipation in terms of the ligaments plasticity and fracture due to increasing bondline thickness contributes more to the total energy release, thus establishing an increasing trend in fracture toughness. However, once the bondline thickness exceeds a threshold value, the added dissipation from increasing bondline thickness is no longer enough to compensate for the dissipation loss due to the reduction of bridging ligaments; thus, the system features a decline in toughness at a decaying rate. Increasing the adhesive thickness further leads to a pure interfacial fracture without any crack-tip transfer, and the dissipation will be purely from the interfacial fracture. Then the fracture toughness is therefore not evidently changed, and approximately equals to the SERR of the surface debonding between substrate and adhesive. According to our analysis, the plasticity of adhesives plays a significant role in the toughness of bonded joints, which is in accordance with Ji et al. (2010), where the influence of the plastic dissipation in the toughened adhesive interlayer was described as the mechanism responsible for the bondline thickness dependence. Liao et al. (2013) found that the toughness of ABJs increases as the adhesive thickness increases for a ductile adhesive, but the trend is opposite for a brittle adhesive. This is possibly due to the fact that, with the increase of the bondline thickness, the bridging ligaments will reduce, and the dissipation from ligaments brittle failure is also relatively low, which is not enough to compensate for the decreased dissipation due to the reduction of ligaments. Based on the above discussion, an optimum bondline thickness may be achieved depending on the stochastic characteristics, adhesive properties, geometrical parameters, and also loading types. This analysis highlights the potential of maximizing toughness by optimizing the adhesive thickness in design process. Apart from the interpretation we explored in this work, the bondline thickness effect may also be attributed to other factors such as defects (Arenas et al., 2010) and singular stress field (Noda et al., 2007), *etc.*

## 5. Parametric study on the stochastic interfacial properties

Due to the variability in the quality of manufacture and surface pre-treatment, bonding interfaces may possess different statistic characteristics, which is believed to endow FRP joints with different enhanced toughness. For the purpose of thoroughly understanding the sensitivity of bonding performance of FRP joints to the parameters of interfacial variability, we carried out a parametric study.

### 5.1. Effect of standard deviation $\sqrt{\mathrm{Var}\,(\sigma_m)}$

Keeping $G_c$ deterministic without any variance, we performed five groups of simulations with different standard deviations of $\sigma_m$, which were $\sqrt{\mathrm{Var}\,(\sigma_m)} = 0.60$, 1.20, 1.80, 2.40, and 3.03. In the following simulations, the means of ($\sigma_m$,$G_c$) are in accordance with the values in Table 1.

Fig. 9 presents the statistical results. The model subjected to $\sqrt{\mathrm{Var}\,(\sigma_m)}$ =0.60 debonded without any ligament, the obtained $G_c$ was close to that of the reference model. We observe an almost linear relationship between the number of ligaments and $\sqrt{\mathrm{Var}\,(\sigma_m)}$. Crack-tip is more likely to transfer from one interface to another for the model subjected to larger $\sqrt{\mathrm{VAR}\,(\sigma_m)}$ during the debonding process, and thus more ligaments tend to be built. The toughening of ABJs has been proven by the improved capability of debonding resistance for all the tested cases with bridging ligaments. A monotonous increase of $G_c$ at a decaying rate

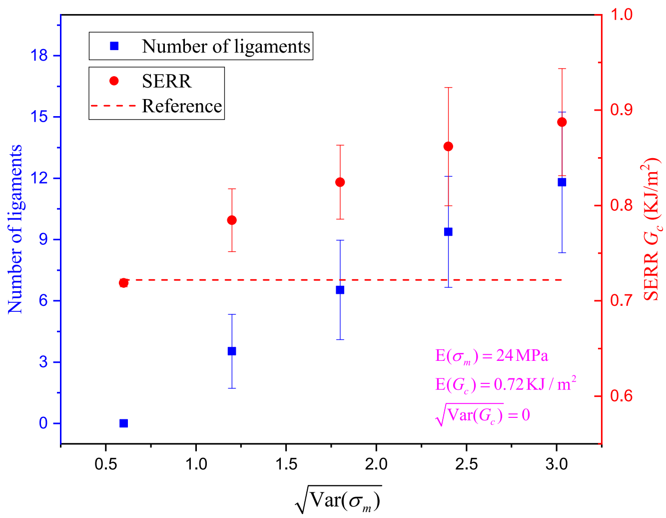


**Fig. 9.** Scatter plot of ligament number and the average SERR obtained by the models with different $\sqrt{\text{Var}\,(\sigma_m)}$. ($t_a = 0.15$ mm).

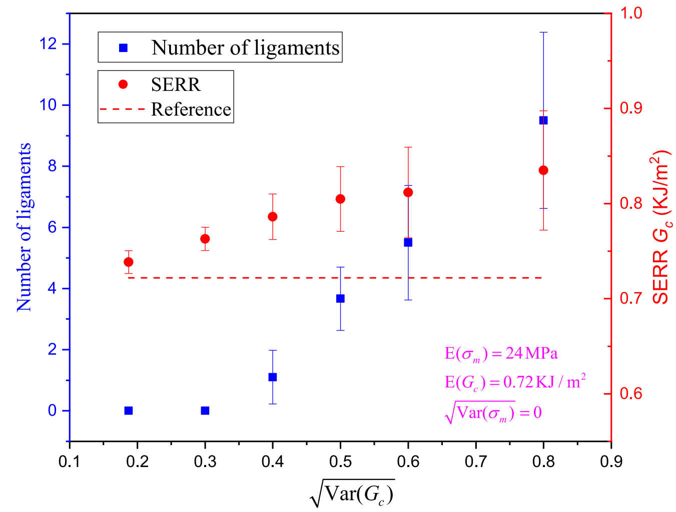


**Fig. 10.** Scatter plot of ligament number and the average SERR obtained by the models with different $\sqrt{\text{Var}\,(G_c)}$. ($t_a = 0.15$ mm).

is observed with the increase of $\sqrt{\text{Var}\,(\sigma_m)}$. For the debonding propagating from $\Delta a = 0$ to $\Delta a = 55$ mm, the model with deviation $\sqrt{\text{Var}\,(\sigma_m)} = 3.03$ features the maximum toughness enhancement, for which the total energy dissipation is approximately 22.9% higher compared to the reference model with uniform bonding properties, as shown in Fig. 9. In general, the model subjected to greater variability in $\sigma_m$ will build up more ligaments and thus produce more extrinsic dissipation.

### 5.2. Effect of standard deviation $\sqrt{\text{Var}\,(G_c)}$

Keeping $\sigma_m$ deterministic, *i.e.*, $\sqrt{\text{Var}\,(\sigma_m)} = 0$, we performed model runs with different standard deviations of $G_c$, *i.e.* $\sqrt{\text{Var}\,(G_c)} = 0.19$, 0.30, 0.40, 0.50, 0.60 and 0.80, to help elucidate the sensitivity of joints toughness to $G_c$. Crack-tip transfer did not occur in the models with $\sqrt{\text{Var}\,(G_c)} = 0.19$ and 0.30, whereas the other models experienced crack-tip transfer and ligament bridging. Similarly, a critical value of $\sqrt{\text{Var}\,(G_c)}$ exists, above which, crack-tip transfer can happen, and thus establishing ligament bridging. Obvious enhancement in joints' toughness was observed for all the cases, as indicated by the predictions shown in Fig. 10. Theoretically, in simulations, the measured SERR of the model without crack-tip transfer should be equivalent to the mean value of the randomly generated SERR of the debonding interface (close to the reference value). However, as per the predictions we obtained, the measured toughness of the models with pure interfacial fracture is higher than the reference value. This can be explained by the fact that the undebonding interface also underwent interfacial failure, which released non-negligible amounts of energy, although with no apparent fracture. The toughness of joints with $\sqrt{\text{VAR}\,(G_c)}$ greater than the threshold ($\sqrt{\text{Var}\,(G_c)} = 0.50$ in the present case) is not sensitive to the increasing $\sqrt{\text{Var}\,(G_c)}$ and the systems tend to dissipate a similar amount of energy for the same crack extension, *i.e.*, possess similar fracture toughness. This is counterintuitive and different from the sensitivity of $\sqrt{\text{Var}\,(\sigma_m)}$ on the toughening effect of FRP joint. This is possibly due to the fact that the crack-tip tends to transfer into the interface with lower $G_c$, even when the number of ligaments is increased with increasing $\sqrt{\text{Var}\,(G_c)}$, and the decreased dissipation due to the weak interface and the additional are approximately equivalent.

### 5.3. Effect of correlation coefficients $\rho$

The correlation coefficient $\rho \in [-1, 1]$, in Eq. (3), indicates the strength of the statistical relevance between $\sigma_m$ and $G_c$. To fully understand the effect of the correlation coefficient on the bonding performance of the composite joint, we investigated both negative correlation and positive correlation. In total, we performed five groups of simulations, with five different correlation coefficients $\rho = -1$, $-0.5$, 0, 0.5 and 1. The generated stochastic bonding properties for different correlation coefficients are shown in Fig. 11. A correlation of $-1$ shows a perfect negative correlation, while a correlation of 1 shows a perfect positive correlation. A correlation of 0 shows no relationship between the variations of $\sigma_m$ and $G_c$, *i.e.*, the two properties are independent.

Fig. 12 shows how the correlation influences the number of ligaments and the effective toughening. Overall, the toughness of joints and the number of ligaments formed during debonding demonstrated opposite trends when $\rho$ is varied. In case of positive correlation, low strength and low toughness tend to be at the same spatial point as indicated in Fig. 11a and b. On the contrary, the point possesses low strength and high toughness in case of negative correlation as indicated in Fig. 11d and e. The initiation of crack-tip transfer occurs more easily with positive $\rho$: the probability of ligament bridging is higher compared to those joints with negative $\rho$, as proved by the variation of ligaments' number in Fig. 12. However, despite there are more bridging events when increasing $\rho$, these bridging events are individually less efficient in dissipating energy, as the toughness reduces together with the strength. The "weak strength" activated bridging events are also "low toughness" events. On the contrary, for negative $\rho$, fewer but more efficient events can be observed as the "weak strength" events come with high toughness due to the negative correlation coefficient. These two mechanisms are competing, one increasing the effective toughness with the correlation, the other one decreasing the effective toughness with the correlation. These two effects offset each other, except for correlation close to $-1$ for which the efficient of individual ligaments seems to be the preponderant effect.

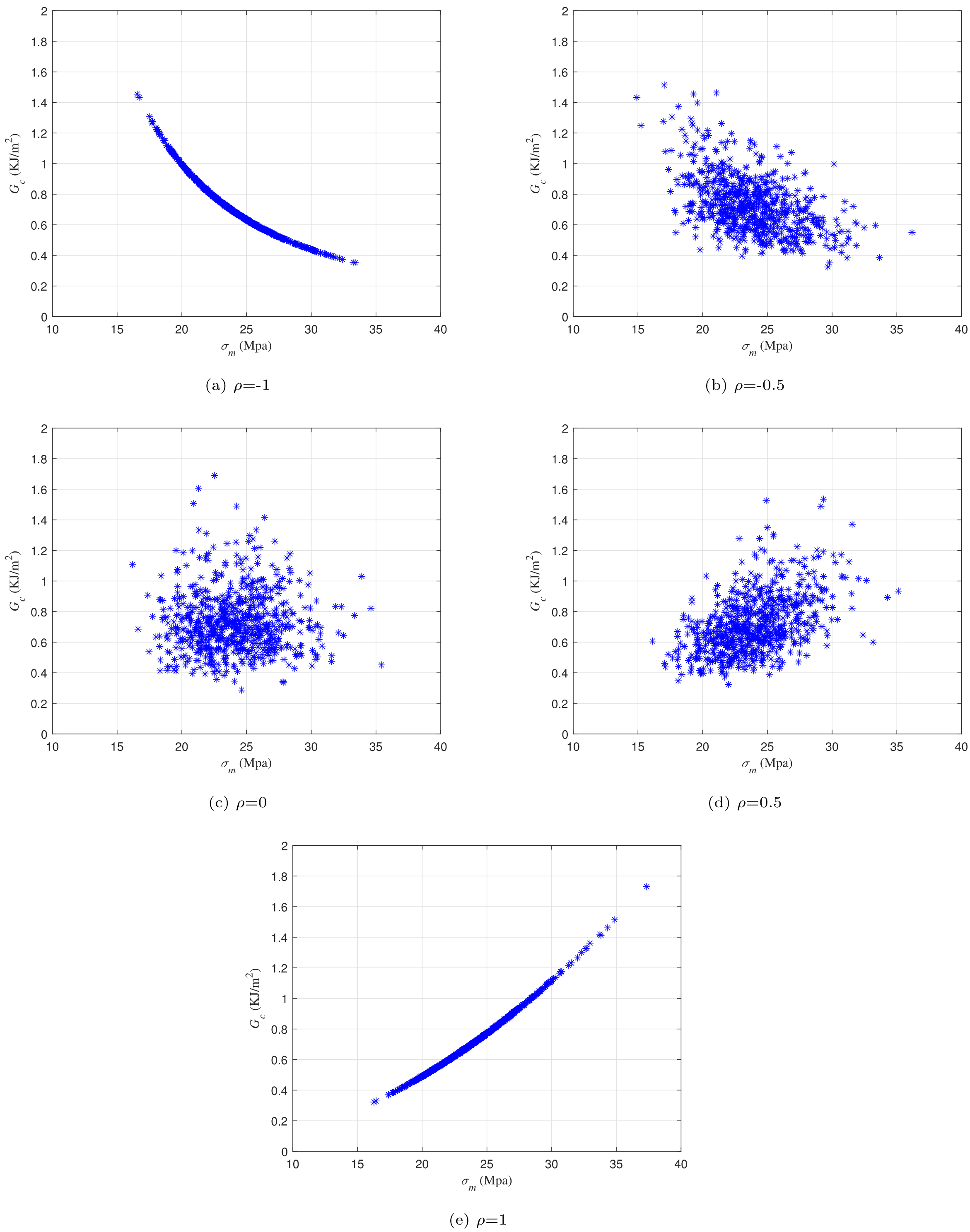


**Fig. 11.** Scatter plot of the generated pairs of ($\sigma_m$, $G_c$) subjected to different correlation coefficients.

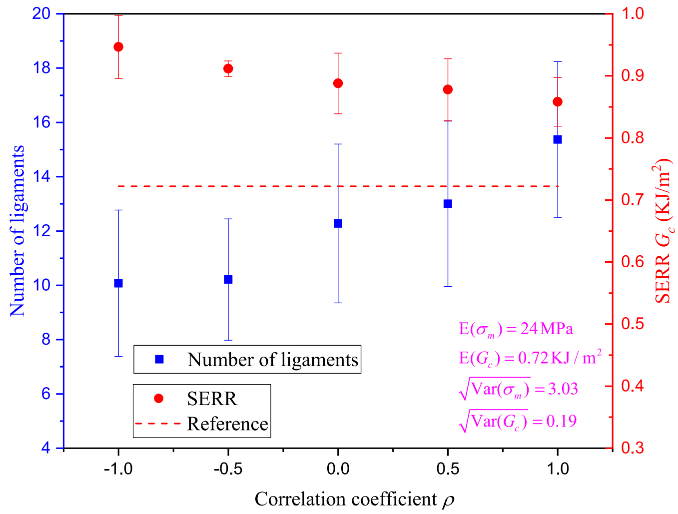


**Fig. 12.** Scatter plot of ligament number and the average SERR obtained by the models with different $\rho$. ($t_a = 0.15$ mm).

## 6. Conclusions and closing remarks

The physical debonding mechanisms of FRP ABJs subjected to a variability in interfacial properties are elaborated by applying a newly developed modeling strategy. Based on the results and discussion, we can draw the following conclusions:

(1) By applying the developed modeling strategy, we have captured the mechanisms of crack-tip transfer and ligament bridging during the debonding of FRP ABJs, which confirms that our modeling strategy is applicable and practical.
(2) The spatially distributed stochastic properties of the interface significantly influence the debonding behaviors of FRP joints by triggering the mechanisms of crack-tip transfer and ligament bridging. Consequently, an enhancement in crack resistance of composite joints is achieved, in terms of extrinsic dissipation contributed from the extra debonding surface and the plastic deformation and failure of adhesives, leading to a tougher and more robust joint system.
(3) Crack-tip transfer and the associated ligament bridging can be one of the main mechanisms responsible for the bondline thickness effect on fracture toughness of ABJs. It appears that an optimum bondline thickness exists for bonding adhesion subjected to specific stochastic characteristics, with which the performance of ABJs is expected to be maximized.
(4) Our parametric study reveals that the toughness of FRP ABJs is sensitive to the parameters of stochastic distribution. Greater standard deviations of $\sigma_m$ and $G_c$ tend to build up more ligaments, which may provide more extrinsic dissipation and significantly influence the structure response, and more importantly, the toughness of a joint. The variation of correlation coefficient $\rho$ activates two competitive mechanisms that more bridging events occur when increasing $\rho$ while these bridging events are individually less efficient in dissipating energy.
(5) The results point the way to improve design of innovative FRP ABJs, during the debonding of which, large-scale ligament bridging can be controlled, and thus the extrinsic dissipation may be explored to enhance the performance of ABJs.

All the results presented here were performed under pure mode-I condition. In the future, the proposed numerical modeling strategy will be applied to investigate the effect of variability in interfacial properties of ABJs under mode-II and mixed-mode loading, which is more significant and generalized. Future works will also focus on turning these observations into new approaches for the design of adhesive joints. As we demonstrated that heterogeneous bonding properties can strongly affect the interface and that this effect is dependent on the thickness of the interface, we can now design both the substrate heterogeneity (using appropriate treatment such as lasers for example) and the geometry of the joint to tailor the relative weight of local and non-local dissipation mechanisms.

## Declaration of Competing Interest

The authors declare that they have no known competing financial interests or personal relationships that could have appeared to influence the work reported in this paper.

## CRediT authorship contribution statement

**Xiaole Li:** Conceptualization, Methodology, Visualization, Data curation, Formal analysis, Writing - review & editing. **Ran Tao:** Visualization, Data curation, Formal analysis, Writing - review & editing. **Marco Alfano:** Data curation, Formal analysis, Writing - review & editing. **Gilles Lubineau:** Conceptualization, Supervision, Project administration, Methodology, Data curation, Formal analysis, Writing - review & editing.

## Acknowledgments

The research reported in this publication was supported by funding from King Abdullah University of Science and Technology (KAUST) Office of Sponsored Research (OSR) under award number OSR-2017-CRG6-3388.01.

## References

Arenas, J.M., Narbon, J.J., Alía, C., 2010. Optimum adhesive thickness in structural adhesives joints using statistical techniques based on weibull distribution. Int. J. Adhes. Adhes. 30 (3), 160–165.
Ashcroft, I.A., Khokar, Z.R., Silberschmidt, V.V., 2012. Modelling the effect of microstructural randomness on the mechanical response of composite laminates through the application of stochastic cohesive zone elements. Comput. Mater. Sci. 52 (1), 95–100.
Azari, S., Papini, M., Spelt, J.K., 2011. Effect of adhesive thickness on fatigue and fracture of toughened epoxy joints part I: experiments. Eng. Fract. Mech. 78 (1), 153–162.
Balakrishnan, N., Lai, C.D., 2009. Continuous Bivariate Distributions. Springer Science & Business Media.
Berry, J.P., 1963. Determination of fracture surface energies by the cleavage technique. J. Appl. Phys. 34 (1), 62–68.
Blaysat, B., Hoefnagels, J.P., Lubineau, G., Alfano, M., Geers, M.G., 2015. Interface debonding characterization by image correlation integrated with double cantilever beam kinematics. Int. J. Solids Struct. 55, 79–91.
Boutar, Y., Naïmi, S., Mezlini, S., da Silva, L.F., Hamdaoui, M., Ben Sik Ali, M., 2016. Effect of adhesive thickness and surface roughness on the shear strength of aluminium one-component polyurethane adhesive single-lap joints for automotive applications. J. Adhes. Sci. Technol. 30 (17), 1913–1929.
Budhe, S., Banea, M.D., de Barros, S., da Silva, L.F.M., 2017. An updated review of adhesively bonded joints in composite materials. Int. J. Adhes. Adhes. 72, 30–42.
Canal, L.P., Alfano, M., Botsis, J., 2017. A multi-scale based cohesive zone model for the analysis of thickness scaling effect in fiber bridging. Compos. Sci. Technol. 139, 90–98.
Canal, L.P., Pappas, G., Botsis, J., 2016. Large scale fiber bridging in mode I intralaminar fracture. an embedded cell approach. Compos. Sci. Technol. 126, 52–59.
Carlberger, T., Stigh, U., 2010. Influence of layer thickness on cohesive properties of an epoxy-based adhesivean experimental study. J. Adhes. 86 (8), 816–835.
Cheng, Y.-S., 1986. Bivariate lognormal distribution for characterizing asbestos fiber aerosols. Aerosol Sci. Technol. 5 (3), 359–368.
Dimas, L.S., Giesa, T., Buehler, M.J., 2014. Coupled continuum and discrete analysis of random heterogeneous materials: elasticity and fracture. J. Mech. Phys. Solids 63, 481–490.
Dimas, L.S., Veneziano, D., Buehler, M.J., 2016. Strength and fracture toughness of heterogeneous blocks with joint lognormal modulus and failure strain. J. Mech. Phys. Solids 92, 72–86.
Dimas, L.S., Veneziano, D., Giesa, T., Buehler, M.J., 2015. Probability distribution of fracture elongation, strength and toughness of notched rectangular blocks with lognormal young's modulus. J. Mech. Phys. Solids 84, 116–129.

Garca-Guzmn, L., Tvara, L., Reinoso, J., Justo, J., Pars, F., 2018. Fracture resistance of 3D printed adhesively bonded DCB composite specimens using structured interfaces: experimental and theoretical study. Compos. Struct. 188, 173–184.
Gowrishankar, S., Mei, H., Liechti, K.M., Huang, R., 2012. A comparison of direct and iterative methods for determining traction-separation relations. Int. J. Fract. 177 (2), 109–128.
Haider, A.-Z., Zhao, X.-L., Al-Mihaidi, R., 2011. Mechanical behaviour of normal modulus carbon fibre reinforced polymer (CFRP) and epoxy under impact tensile loads. Procedia Eng. 10, 2453–2458.
Heide-Jrgensen, S., Teixeira de Freitas, S., Budzik, M.K., 2018. On the fracture behaviour of CFRP bonded joints under mode I loading: effect of supporting carrier and interface contamination. Compos. Sci. Technol. 160, 97–110.
Ji, G., Ouyang, Z., Li, G., 2013. Effects of bondline thickness on mode-I nonlinear interfacial fracture of laminated composites: an experimental study. Compos. Part B 47, 1–7.
Ji, G., Ouyang, Z., Li, G., Ibekwe, S., Pang, S.-S., 2010. Effects of adhesive thickness on global and local mode-i interfacial fracture of bonded joints. Int. J. Solids Struct. 47 (18–19), 2445–2458.
Jumel, J., 2017. Crack propagation along interface having randomly fluctuating mechanical properties during DCB test finite difference implementation evaluation of $G_c$ distribution with effective crack length technique. Compos. Part B 116, 253–265.
Katnam, K.B., Da Silva, L.F.M., Young, T.M., 2013. Bonded repair of composite aircraft structures: a review of scientific challenges and opportunities. Prog. Aerosp. Sci. 61, 26–42.
Kaute, D.A.W., Shercliff, H.R., Ashby, M.F., 1993. Delamination, fibre bridging and toughness of ceramic matrix composites. Acta Metall. Mater. 41 (7), 1959–1970.
Khokhar, Z.R., Ashcroft, I.A., Silberschmidt, V.V., 2009. Simulations of delamination in CFRP laminates: effect of microstructural randomness. Comput. Mater. Sci. 46 (3), 607–613.
Khokhar, Z.R., Ashcroft, I.A., Silberschmidt, V.V., 2013. Three-dimensional analysis of the effect of material randomness on the damage behaviour of CFRP laminates with stochastic cohesive-zone elements. Appl. Compos. Mater. 21 (1), 71–89.
Kinloch, A.J., Shaw, S.J., 1981. The fracture resistance of a toughened epoxy adhesive. J. Adhes. 12 (1), 59–77.
Liao, L., Huang, C., Sawa, T., 2013. Effect of adhesive thickness, adhesive type and scarf angle on the mechanical properties of scarf adhesive joints. Int. J. Solids Struct. 50 (25–26), 4333–4340.
Maloney, K., Fleck, N., 2018. Damage tolerance of an architected adhesive joint. Int. J. Solids Struct. 132–133, 9–19.
Maloney, K., Fleck, N., 2019. Toughening strategies in adhesive joints. Int. J. Solids Struct. 158, 66–75.
Manshadi, B.D., Farmand-Ashtiani, E., Botsis, J., Vassilopoulos, A.P., 2014. An iterative analytical/experimental study of bridging in delamination of the double cantilever beam specimen. Compos. Part A 61, 43–50.
Marzi, S., Biel, A., Stigh, U., 2011. On experimental methods to investigate the effect of layer thickness on the fracture behavior of adhesively bonded joints. Int. J. Adhes. Adhes. 31 (8), 840–850.
Meng, F., Thouless, M., 2019. Cohesive-zone analyses with stochastic effects, illustrated by an example of kinetic crack growth. J. Mech. Phys. Solids 132, 103686.
Mirzaei, B., Sinha, A., Nairn, J.A., 2016. Measuring and modeling fiber bridging: application to wood and wood composites exposed to moisture cycling. Compos. Sci. Technol. 128, 65–74.
Monsef, S.A., Ortega, A., Turon, A., Maim, P., Renart, J., 2019. An efficient method to extract a mode I cohesive law for bonded joints using the double cantilever beam test. Compos. Part B 178, 107424.
Moszner, N., Salz, U., 2007. Recent developments of new components for dental adhesives and composites. Macromol.. Mater. Eng. 292 (3), 245–271.
Motamedi, D., Milani, A.S., Komeili, M., Bureau, M.N., Thibault, F., Trudel-Boucher, D., 2013. A stochastic XFEM model to study delamination in PPS/glass UD composites: effect of uncertain fracture properties. Appl. Compos. Mater. 21 (2), 341–358.
Moyer, D.J.D., Wightman, J.P., 1991. The effect of surface pretreatment on carbon fibre-polyimide matrix composite bonding. Surf. Interface Anal. 17 (7), 457–464.
Nguyen, A.T.T., Brandt, M., Orifici, A.C., Feih, S., 2016. Hierarchical surface features for improved bonding and fracture toughness of metalmetal and metalcomposite bonded joints. Int. J. Adhes. Adhes. 66, 81–92.
Noda, N.-A., Shirao, R., Li, J., Sugimoto, J.-S., 2007. Intensity of singular stress fields causing interfacial debonding at the end of a fiber under pullout force and transverse tension. Int. J. Solids Struct. 44 (13), 4472–4491.
Prolongo, S.G., Gude, M.R., Del Rosario, G., Urea, A., 2010. Surface pretreatments for composite joints: study of surface profile by SEM image analysis. J. Adhes. Sci. Technol. 24 (11–12), 1855–1867.
Sarrado, C., Turon, A., Costa, J., Renart, J., 2016. An experimental analysis of the fracture behavior of composite bonded joints in terms of cohesive laws. Compos. Part A 90, 234–242.
Sills, R., Thouless, M., 2015. Cohesive-length scales for damage and toughening mechanisms. Int. J. Solids Struct. 55, 32–43.
Taleb Ali, M., Jumel, J., Shanahan, M.E.R., 2018. Effect of adhesion defects on crack propagation in double cantilever beam test. Int. J. Adhes. Adhes. 84, 420–430.
Tao, R., Alfano, M., Lubineau, G., 2018. Laser-based surface patterning of composite plates for improved secondary adhesive bonding. Compos. Part A 109, 84–94.
Tao, R., Alfano, M., Lubineau, G., 2019. *in-situ* analysis of interfacial damage in adhesively bonded composite joints subjected to various surface pretreatments. Compos. Part A 116, 216–223.
Tenchev, R.T., Falzon, B.G., 2007. Experimental and numerical study of debonding in composite adhesive joints. In: 16th International Conference on Composite Materials, Kyoto, Japan.
Tzetzis, D., 2008. The role of surface morphology on the strength and failure mode of polymer fibre reinforced single lap joints. J. Mater. Sci. 43 (12), 4271–4281.
Wingfield, J.R.J., 1993. Treatment of composite surfaces for adhesive bonding. Int. J. Adhes. Adhes. 13 (3), 151–156.
Wu, C., Gowrishankar, S., Huang, R., Liechti, K.M., 2016. On determining mixed-mode tractionseparation relations for interfaces. Int. J. Fract. 202 (1), 1–19.
Wu, C., Huang, R., Liechti, K.M., 2019. Simultaneous extraction of tensile and shear interactions at interfaces. J. Mech. Phys. Solids 125, 225–254.
Xu, W., Yu, H.C., Tao, C.H., 2014. Influence of randomly distributed adhesive properties on the overall mechanical response of metallic adhesively bonded joints. Int. J. Adhes. Adhes. 52, 48–56.
Zotti, A., Zuppolini, S., Zarrelli, M., Borriello, A., 2016. Fracture toughening mechanisms in epoxy adhesives. Adhesives-Applications and Properties. IntechOpen.